Publication III

Wade Karlsen, Mykola Ivanchenko, Ulla Ehrnstén, Yuriy Yagodzinskyy, and Hannu Hänninen. 2009. Microstructural manifestation of dynamic strain aging in AISI 316 stainless steel. Journal of Nuclear Materials, volume 395, numbers 1-3, pages 156-161.

Journal of Nuclear Materials 395 (2009) 156–161

Contents lists available at ScienceDirect

Journal of Nuclear Materials

journal homepage: www.elsevier.com/locate/jnucmat

Microstructural manifestation of dynamic strain aging in AISI 316 stainless steel

Wade Karlsen [a,*], Mykola Ivanchenko [b], Ulla Ehrnstén [a], Yuriy Yagodzinskyy [b], Hannu Hänninen [b]

[a] VTT Technical Research Centre of Finland, P.O. Box 1000, FI-2044 VTT, Finland
[b] Helsinki University of Technology, Laboratory of Engineering Materials, P.O. Box 4200, FI-02015 TKK, Finland

ARTICLE INFO

Article history:
Received 26 August 2008
Accepted 9 October 2009

ABSTRACT

Dynamic strain aging (DSA) affects a material's mechanical behaviour. In the current study, the deformation microstructures of AISI 316 stainless steel specimens were examined after tensile testing at several temperatures both in and out of the DSA-regime (200, 288 and 400 °C), and the effect of straining on free nitrogen evolution at those temperatures was studied by Anelastic Mechanical Loss Spectrometry (Internal Friction). Analysis of the nitrogen-induced Snoek-like peak after straining indicated that DSA behaviour is associated with the formation of sub-micron scale, nitrogen-enriched zones in the austenitic matrix. Long-range planarity was observed in the dislocation structures at 400 °C and short-range planarity at 288 °C, but at 200 °C the microstructure exhibited cellular dislocation structure. Diffusion re-distribution of nitrogen in the DSA-regime affected the deformation behaviour of the material by restricting cross-slip, which in turn promotes strain localization, degrading the mechanical performance of the material.

1. Introduction

Dynamic strain aging (DSA) is a material phenomenon most commonly associated with the appearance of serrations in the tensile stress–strain curves at particular test temperatures. Rather than random inflections in the curve, the serrations have been found to be regular, repeatable, and even separable into particular types [1]. DSA is important to structural stainless steels because it is associated with the anomalous evolution of strength and ductility with temperature, both for tensile and fatigue tests [2]. Rather than a consistent decline in strength with increasing temperature, some materials show a retardation or even reversal of that decline at some temperatures, which is attributed to DSA. Likewise, a ductility minimum occurs in the same temperature range [3,4]. The temperature of DSA occurrence is material dependent, e.g. for low-alloy RPV steel serrations are observed at 140–340 °C [5], while for austenitic stainless steels they occur in the range 300–650 °C [6]. Cold-working prior to tensile testing promotes the appearance of serrations. There is also a strong effect of strain rate on the incidence of DSA, such that reducing the strain rate broadens the range of the incidence of serrations and brings it to lower temperatures (conversely, increasing the strain rate can suppress DSA's appearance) [6].

The aforementioned are behaviours that are attributed to the DSA phenomenon. The mechanism underlying the DSA phenomenon is typically considered to be the impedance of dislocation glide by their interaction with diffusing solute atoms [7,8]. At lower temperatures the culprit is typically deemed to be interstitial atoms (C, N, B), while at higher temperatures in stainless steels, substitutional Cr has been considered responsible [3].

Testing of the DSA mechanism hypothesis has been approached from many angles. For example, anelastic mechanical loss spectrometry (internal friction) has been used for measuring the behaviour of the interstitials in austenitic alloys [6]. On the other hand, transmission electron microscopy (TEM) can be used to examine the manifestation of DSA in the microstructure. As the name implies, "dynamic" strain aging is a dynamic process, i.e. it occurs during the application of a rising load. TEM, however, is generally limited to post-mortem examinations. Nonetheless, there has been some TEM work done in conjunction with some DSA studies [3]. The results indicate that the altered mechanical behaviours observed in the regime of DSA are typically associated with a more planar microstructure, as opposed to a cellular one. Such planarity is particularly stark for material fatigue-loaded in vacuum. For materials fatigue-tested in the DSA temperature regime, a structure referred to as "corduroy" has been observed. Corduroy, as its name implies, is comprised of narrowly-spaced stripes of contrast, which is an extreme case of unidirectional dislocation alignment [9].

The results of a broader study mapping the DSA behaviour of AISI 316 stainless steels having several different nitrogen contents, over a range of strain rates, temperatures and levels of prior cold work, have been reported in [10]. The goal of the current study was to examine the deformation microstructures and internal friction response of a sub-set of those test materials, in order to determine any observable differences in the resulting dislocation structures and internal friction response of materials showing

* Corresponding author. Tel.: +358 20 722 6865; fax: +358 20 722 7002.
E-mail address: wade.karlsen@vtt.fi (W. Karlsen).

0022-3115/$ - see front matter © 2009 Elsevier B.V. All rights reserved.
doi:10.1016/j.jnucmat.2009.10.047

and not showing DSA behaviour, to enable the interstitial atom behaviour to be linked with the deformation behaviour.

2. Experimental

The material of this study was a solution annealed commercial AISI 316 NG stainless steel with the following composition (in wt.%): Cr, 17.0; Ni, 12.5; Mo, 2.28; Mn, 1.66; Si, 0.38; Cu, 0.11; N, 0.093; C, 0.022; P, 0.027; Fe, balance. It originated from a short section of a pipe that was manufactured for use in a nuclear reactor. To prepare tensile specimens, slices 2 mm in thickness were first cut from the pipe by electric discharge machining (EDM), oriented in the longitudinal direction such that the width of the test bar corresponded to the wall thickness of the pipe. The tensile test specimens were then prepared according to ASTM standard E 8M (sheet-type, sub-size specimens), except that extensions were welded to the specimen ends for fitting more securely in the test machine grips. The weld occurred well outside of the test region and would not influence the test results.

Tensile tests were performed according to standard SFS-EN 1002–1 and ASTM standard E21, using a 25 kN MTS 858 test machine equipped with an MTS High-Temperature Furnace 653.02. A strain rate of $10^{-5}\,s^{-1}$ was employed, and tests were carried out at four different temperatures: 26, 200, 288 and 400 °C. The cooling time to 26 °C after the straining at elevated temperatures did not exceed 2 min.

The internal friction (IF) method was used to indicate the presence of the free nitrogen and its diffusive re-distribution in the crystalline lattice of the material. Specimens for IF measurements were taken from the gauge lengths of tensile test specimens which had been strained to 20% of elongation at the same strain rate and temperatures as those tested all the way to fracture. The specimens had the typical dimensions of $0.5 \times 1.5 \times 45$ mm, and were prepared by cutting with an abrasive disc saw and then mechanically polishing with 1200 grit emery paper.

The internal friction, Q^{-1}, was measured with an inverted torsion pendulum over the temperature range −170 to 550 °C. The amplitude of the torsion deformation applied by the pendulum to the specimen did not exceed 10^{-5}, the natural frequency of the pendulum varied in the range of 1–2 Hz. The heating rate of the specimens during the IF measurements was 2 °C/min.

Specimens for TEM examination were prepared from the deformed gauge region and adjacent to the fracture surface of each bar tested to fracture. To represent the as-received condition, specimens were also prepared from the grip region of the 400 °C bar, for avoiding the heat-affected zone of the extension weld. Because of the thin sheet geometry of the tensile bars, they were first ground to <0.1 mm thickness, and then 3 mm diameter disk specimens for TEM were punched from the fractured bars in the plane orientation. Those disks were subsequently electropolished to electron transparency with a Tenupol 5 running a 3% perchloric acid/methanol solution at −35 °C and 23–26 V.

3. Results

3.1. DSA manifestation in the studied steel

The typical engineering stress–strain curves for the AISI 316 NG steel containing 0.093 wt.% nitrogen are shown in Fig. 1 for all three elevated testing temperatures (200, 288 and 400 °C). DSA serrations on the stress–strain curves are well-defined at the testing temperatures of 288 and 400 °C, while at 200 °C they are absent in the whole range of the strain, all the way through to fracture. In the test at 288 °C, the onset of serrations of type A, which are periodic abrupt small changes in stress from repeated deformation bands, were observable at an engineering strain of about 0.2 mm/mm. In the test conducted at 400 °C, serrations in the flow stress occurred already from the beginning of plastic straining. The amplitude of the serrations in that test increased with strain and they changed in series from A to A + B type, and just before necking, to mainly B-type serrations, which are oscillations about general level of the stress–strain curves that occur in quick succession [1].

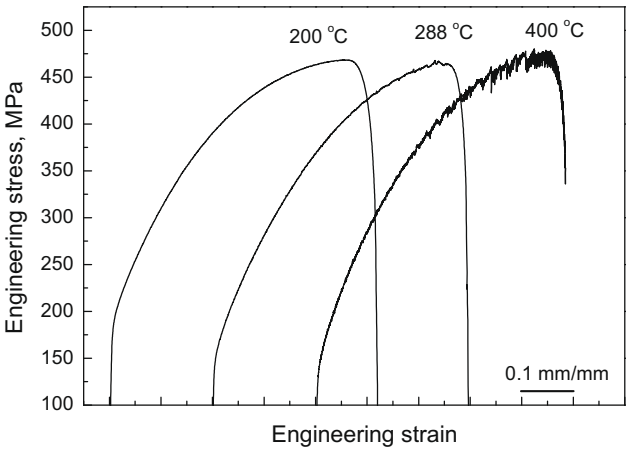

Fig. 1. The stress–strain curves of AISI 316 NG steel tested at $10^{-5}\,s^{-1}$ showing serrated behaviour at 288 and 400 °C, but not at 200 °C, from [10].

3.2. Internal friction measurements

The temperature dependency of the anelastic mechanical energy loss, Q^{-1} (i.e. internal friction), of the material is shown in Fig. 2, for both the as-supplied state and following the pre-straining at 26, 200, 288 and 400 °C. Three well-defined maxima in the Q^{-1} value are apparent for the strained materials, forming peaks situated at about −50, 100 and 350 °C, while only minor fluctuations were evident for the as-supplied material at the corresponding temperatures. The two lower temperature maxima in the Q^{-1} value (at −50 and 100 °C) generally markedly increase in magnitude with the amount of prior cold deformation [11], and are even observed in interstitial-free austenitic stainless steels, such as AISI 316L [12]. They are typically considered to be a consequence of an anelastic response of dislocations interacting with point defects in-

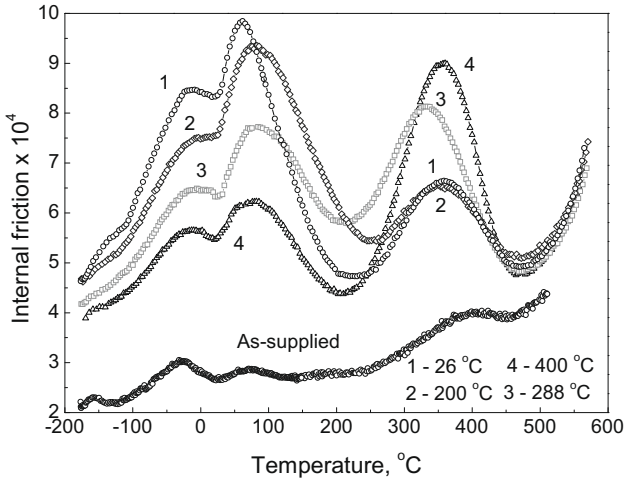

Fig. 2. Internal friction vs. temperature of AISI 316 NG steel after pre-straining (20%) at different temperatures.

duced by cold deformation. Origin of these peaks was analyzed in detail in [12]. The IF peak in the vicinity of 350 °C represents Snoek-like relaxation process, which is known for steels as Finkelshtein–Rosin relaxation [13], and was confirmed by numerous authors in different fcc alloys and pure metals [14]. The last IF peak is the focus of interest in the present study.

The results in Fig. 2 indicate that pre-straining of the material led to a remarkable increase in the peak height, which is associated with nitrogen atoms in the austenite lattice. Moreover, the effect was greater for the pre-straining temperatures above 200 °C. At the same time, the height of the other two IF peaks at lower temperatures decreased with the pre-strain temperature, which is probably a consequence of a recovery of the defects introduced by the pre-straining.

The heights of the Snoek-like IF peaks following background extraction are summarized in Fig. 3 as a function of the pre-straining temperature. In comparison to the as-supplied (annealed) state of the material, some increase in the peak height occurred after pre-straining at room temperature and 200 °C, but the increase is dramatic for 288 and 400 °C, the temperatures at which serrations were present in the tensile tests.

The enhanced nitrogen Snoek-like peak obtained after pre-straining at DSA conditions is unstable. The peak height decays with annealing at temperatures in vicinity of the peak maximum as shown in Fig. 4. The temperature position of the enhanced peak shifts with annealing to the temperature of the peak maximum in as-supplied state. Thus, temperature of the annealing was gradually increased in order to follow the decay of the peak maximum. The peak annealing process can be described by an elemental exponential decay function (shown by dashed line in Fig. 4) with characteristic decay time of 9.3 ± 0.6 ks. The asymptotic value of this decay equals to $(3.5 \pm 0.2) \times 10^{-4}$, which corresponds to the peak height in annealed state of the material (Fig. 2).

3.3. TEM-observations

The non-deformed material was taken from the test bar grip. As shown in Fig. 5, it displayed a moderate density of dislocations. The dislocations were arranged in tangles, but most were quite straight, so in a low-energy state. There were also very few stacking faults visible. Following tensile testing at 200 °C, the dislocation density was much greater. As shown in Fig. 6, the microstructure in that material was comprised of small, thick-

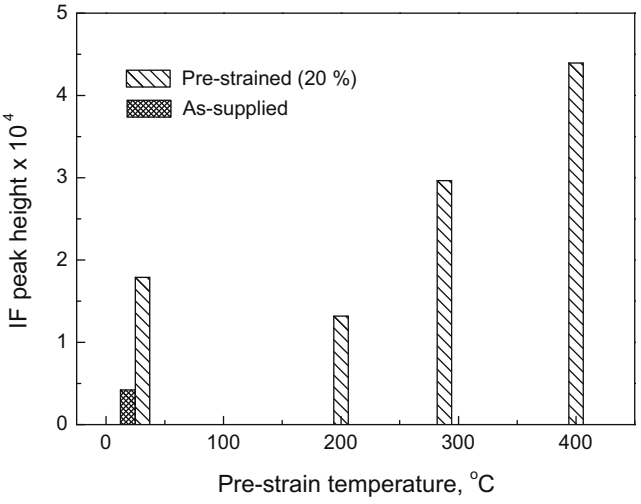

Fig. 3. Amplitudes of the nitrogen Snoek-like peak after IF-background subtraction for different pre-straining temperatures.

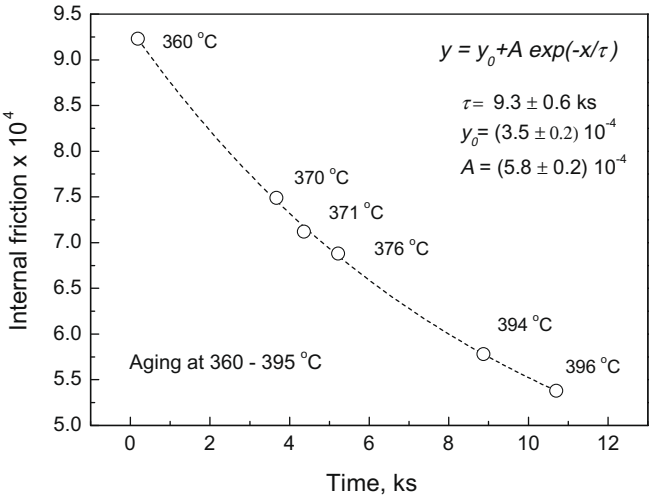

Fig. 4. Snoek-like peak amplitude decay with annealing in vicinity of the Snoek-like peak maximum. The annealing temperature was gradually increased in order to follow migration of the peak maximum occurred during annealing. The decay fits well by exponential decay with characteristic time τ and asymptotic y_0 value shown in the plot.

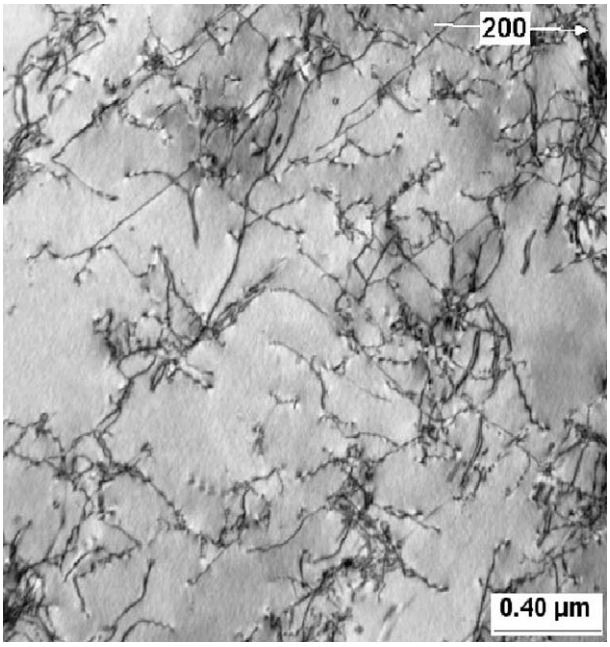

Fig. 5. The microstructure from the non-deformed grip region of the 400 °C bar. Arrow indicates g-vector. Beam is parallel to $[102]_\gamma$.

walled cells. Cellularization is a result of mutual annihilation of dislocations, and the reorganization of remaining dislocations into a lower energy structure. It is enabled by cross-slip, i.e. a dislocation gliding on multiple planes simultaneously. As shown in Fig. 7, the microstructure following tensile testing at 400 °C showed much more linearity than that at 200 °C. That is a consequence of dislocation glide occurring on particular planes. According to DSA theory, the interaction between dislocations and solute atoms limits the freedom of motion of the dislocations; i.e. by pinning portions of the dislocations, the dislocations' ability to cross-slip is restricted. That produces planar slip, which is manifested as linear microstructures. The images in Fig. 8 illustrate the fact that, following tensile testing at 288 °C, the microstructure shows neither a clear cell structure like that at 200 °C, nor long, straight dis-

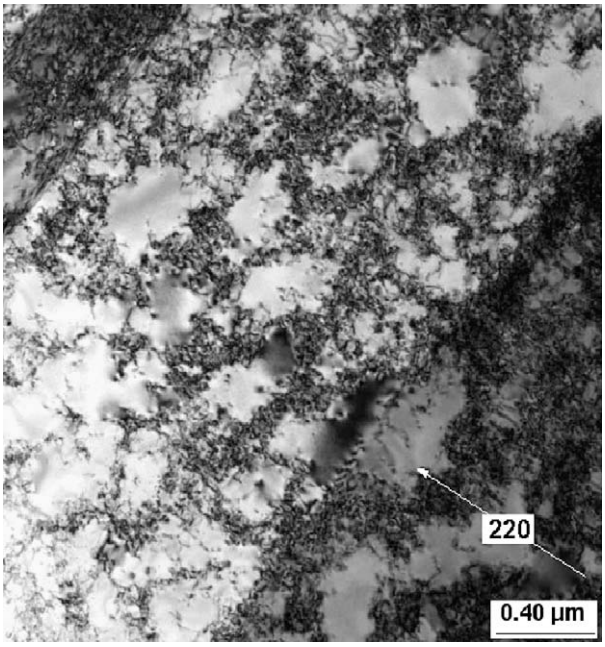

Fig. 6. The microstructure from the gauge region following tensile testing at 200 °C. Arrow indicates g-vector. Beam is parallel to $[100]_\gamma$.

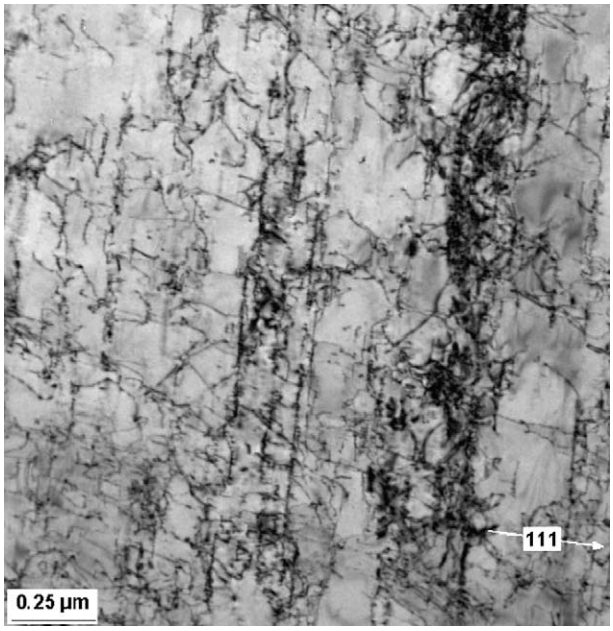

Fig. 7. The microstructure from the gauge region following tensile testing at 400 °C. It shows much more linearity than that at 200 °C. Arrow indicates g-vector. Beam is parallel to $[110]_\gamma$.

locations as at 400 °C. Nonetheless, some orientation is evident, and as the higher magnification image in Fig. 9 shows better, the deformation structure includes a lot of straight dislocation segments that tend to be parallel to each other, another indication of a tendency towards planarization.

In the necked region of the gauge close to the fracture, bands of epsilon martensite were present. They were especially prevalent after the 200 °C test, but were also present after the 288 and 400 °C tests. Examples of such epsilon bands following the 200 °C test are shown in Fig. 10. By imaging the bands in dark-field, it is evident that they are composed of overlapping stacking faults.

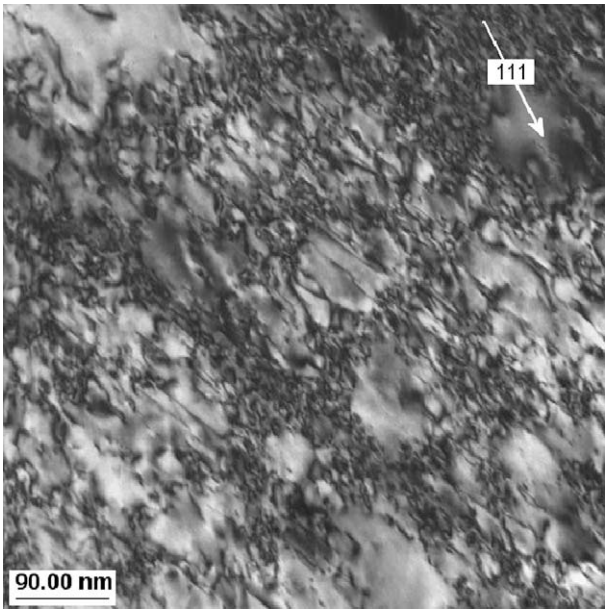

Fig. 8. The microstructure from the deformed gauge region following tensile testing at 288 °C. Arrow indicates g-vector. Beam is parallel to $[110]_\gamma$.

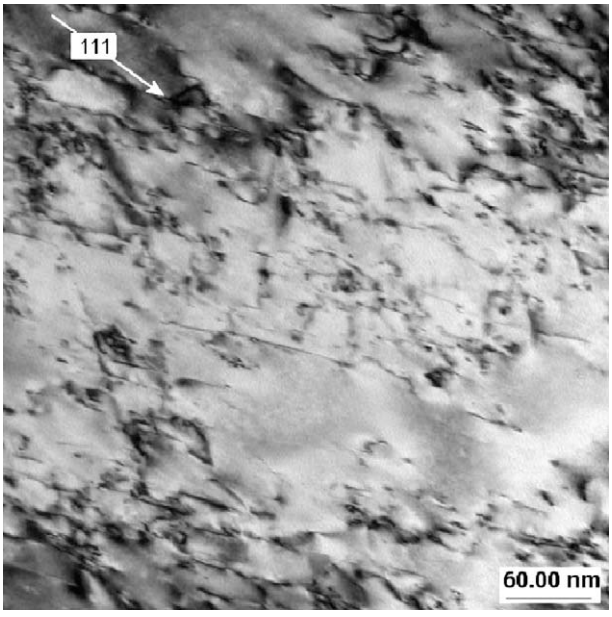

Fig. 9. The 288 °C deformation microstructure viewed at higher magnification. Arrow indicates g-vector. Beam is parallel to $[110]_\gamma$.

The presence of such bands was grain-specific, indicating a difference in the local critical-resolved shear stress, and therefore deformation in neighbouring grains. The necked region of the gauge length reaches a higher stress level, so the critical-resolved shear stress in some grains can reach a high enough stress to promote stacking fault formation by forcing the partial dislocations apart, as described by Hong et al. [4].

4. Discussion

The original model of the relaxation suggested by Verner [15] was based on the mechanism of interstitial–interstitial (*i*–*i*) atom pair re-orientation. This model predicts, in agreement with the

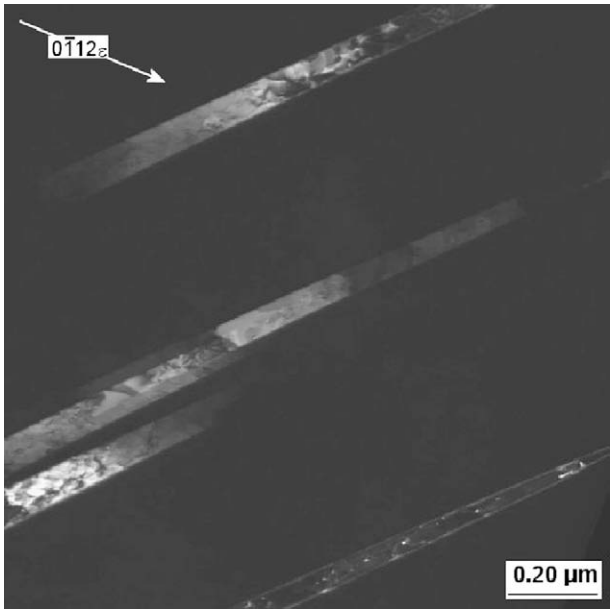

Fig. 10. Dark field image of an example of bands of epsilon martensite visible in the necked region close to the fracture in the 200 °C deformed test bar. Image utilized the reflection having the g-vector indicated, near a beam direction $[0\,1\,\bar{1}\,1]_\varepsilon$.

experimental data, square and linear dependence of the peak height on interstitial atoms concentration when the concentration is low and high, respectively. Several models have been suggested for this relaxation process based on re-orientation of interstitial–substitutional (i–s) atoms and interstitial atom–vacancy (i–v) pairs re-orientation [14,16,17]. Alternative explanation of Snoek-like peak, suggested in [18,19], assumes that the relaxation is caused by re-orientation of a single interstitial, which induces in the lattice of stainless steel non-cubic elastic distortions.

Assuming that the Snoek-like peak amplitude is proportional to nitrogen concentration in the solid solution, and pre-straining of the studied austenitic stainless steel results in a remarkable increase in the magnitude of the Snoek-like peak, one can assume that plastic deformation increases the free nitrogen in the steel lattice. There are three possible sources that may provide the free nitrogen in the steel solid solution during plastic deformation: dislocations pinned by nitrogen atoms, grain boundaries with nitrogen segregation, and nitride particles. Because the material of the study was supplied in the annealed condition and with only a minor amount of nitrides, pinned dislocations and nitride particles are unlikely to be a significant source of free nitrogen. Because of relatively large grain size, which is about 75 μm, the grain boundaries in the material are estimated to be able to contain no more than about 0.01 wt.% of nitrogen (it is assumed here that nitrogen can fully occupy the segregation positions at grain boundaries, the mean atomic portion of which can be estimated as $3h/d$, where $h \approx 1$ nm is the grain boundary thickness and d is the grain size.). Nonetheless, its release by plastic deformation cannot account for the observed twofold increase in the nitrogen peak, considering that the bulk content in the steel is 0.093 wt.%. Thus, some additional mechanism should be taken into account. Additional relaxation due to re-orientation of i–i or i–s pairs formed during straining cannot be considered as the major mechanisms due to high Cr content of the studied steel (17 wt.%) and transitional nature of the enhanced peak. Also, it is hard to expect peak increase due to formation of extra i–v pairs after the deformation at 288 and 400 °C, as low-temperature IF peaks attributed to point defects–dislocation interactions and annihilation of point defects [12] show opposite behaviour to Snoek-like peak (Fig. 2).

An alternative explanation for the observed peak increase lies in the Snoek-like peak origin suggested for austenitic stainless steels in [18], and atomic short-range ordering in substitutional alloys [20]. In multicomponent alloys, interstitial atoms interact with the alloying elements differently. From other side, octahedral interstitial sites are non-equivalent due to different combination of substitutional atoms forming the site [20]. Thus, the symmetry of the local coordination shells around interstitial atom can be lower than cubic, giving rise to elastic dipoles. Due to the higher affinity to chromium atoms in the austenitic stainless steels, nitrogen atoms prefer to occupy the octahedrons with more chromium atoms at the vertices, with the energetically most favourable ones being those with 6 chromium atoms. Interstitial octahedral sites with 6 equivalent substitutional atoms at the octahedron vertices do not take part in the Snoek-like relaxation process, due to the cubic symmetry of the octahedron [21]. Those interstitial positions of high symmetry shield a part of the nitrogen atoms from the Snoek-like relaxation, with the extent of such shielding depending on the short-range ordering of the substitutional atoms in the steel. This in turn can be characterized by the particular fraction of the octahedra having 6 chromium atoms at the vertices [18,20]. The plastic straining of the materials prior to IF measurements changes the substitutional atomic short-range order, which reduces the fraction of high symmetry positions occupied by nitrogen atoms, thereby revealing the presence of the nitrogen interstitials formerly hidden there [22]. That in turn is then manifested as a portion of the increase in the Snoek-like peak height with respect to the annealed condition.

The remaining increase of the peak height following plastic deformation may be a consequence of long-range re-distribution of nitrogen atoms by dislocation dragging, which results in the formation of nitrogen-enriched zones in the lattice. Such zones are of dynamic origin, forming with the deformation-induced dislocation pile-ups and their re-configurations, and are central to DSA. The enrichment of nitrogen in those zones, which occurs at the expense of the nitrogen atoms coming from the shielded sources, like interstitials in octahedra with 6 Cr atoms, and may also increase the fraction of nitrogen atoms taking part in the anelastic relaxation process measured by the IF method.

The nitrogen-enriched zones may occur between dislocation pile-ups, forming dipole-like configurations, where the austenite lattice suffers a remarkable dilatation. Dynamic trapping of nitrogen to those zones can stabilize the opposite pile-ups, and in turn, it can result in growth of the pile-ups, which is manifested in TEM-observations as sub-micron scale strain localization having a planar character.

The peak decay process during annealing at the peak temperature reflects the re-distribution of the free nitrogen that had formed enriched and depleted zones in the austenite lattice in the course of the straining. Analyses of the fine structure of Snoek-like peak showed that diffusing interstitial atoms in lattice of austenitic stainless steel perform up to tens of diffusion jumps each second at the peak temperature [23]. Thus, the characteristic time of the peak decay of 9.3 ks corresponds to amount of diffusion jumps N in the range of 10^4–10^5 with a characteristic diffusion scale $d \approx a\sqrt{N} \sim 0.04$–$0.1$ μm, where $a \approx 3.6 \cdot 10^{-10}$ m is the crystal lattice parameter of austenitic stainless steel [24]. Since the nitrogen re-distribution develops as a diffusion drift under internal stresses caused by inhomogeneous concentration distribution, one can assume that the stress-assisted diffusion path of nitrogen may markedly exceed the above-obtained d-values.

A comparison of the microstructures of the test bars strained at 200, 288 and 400 °C reveals some differences. In particular, the material tensile tested at 400 °C showed a greater tendency towards dislocation planarization, manifested as highly linear dislocation structures. That tensile test had also shown serrations in the

tensile stress–strain curves, and a clearly increased Snoek-like peak height. The 288 °C tensile test also showed serrated flow and an increased Snoek-like peak height, and it also displayed a high proportion of straight, parallel dislocations, though it did not show a long-range planarization like that at 400 °C. On the other hand, the 200 °C tensile tested material did not have such straight dislocations, nor had it shown serrated flow, while the Snoek-like peak was not as high as that for 288 or 400 °C. Thus, it would appear that the planarization in the dislocation microstructure correlates with the IF results, and both are correlated with the altered tensile mechanical behaviour observed.

There are also other factors which can produce planarity in a microstructure though. For example, low stacking fault energy (SFE) more readily allows separation of dislocations into pairs of partial dislocations, which produces a stacking fault. However, such stacking faults would be readily visible in the microstructure. In these materials stacking faults were only observed in association with the formation of bands of epsilon martensite, which were mainly present only in some grains in the regions associated with a higher critical-resolved shear stress (especially in the necked region of the bars). They were not correlated with other linear features in the microstructures though. Therefore, although post-mortem TEM cannot directly observe solute atom interactions with dislocations, the linearity clearly observed in the dislocation structures at 400 °C, and somewhat also at 288 °C, in conjunction with the serrations observed in those tensile stress–strain curves and the IF results showing increased free nitrogen activity, would together imply that the mechanism of DSA is operating in the material, principally at 400 °C, but also at 288 °C.

The DSA phenomenon is important to the overall deformation behaviour of stainless steel as a contributor to strain localization. A degree of strain localization can already occur in lower SFE stainless steels such as AISI 304 and AISI 301. When a perfect dislocation splits into a pair of partial dislocations, the resulting stacking fault is then constrained to glide only on its plane of residence (thereby preventing cross-slip on intersecting planes). Likewise, a dislocation pinned by solute atoms has its cross-slip restricted as well. The restriction of freedom for cross-slip localizes the strain to the most active slip planes, which produces planar slip. Such a restriction promotes dislocation pile-ups rather than the mutual annihilation of interacting dislocations, which in turn raises the flow stress. Additionally, nitrogen stabilizes dislocation pile-ups. This produces the added degree of hardening capability that is manifested as retardation in the thermally-induced softening generally observed with increasing temperature in stainless steels experiencing DSA.

5. Conclusions

Internal friction measurements made on AISI 316 NG austenitic stainless steel showed that the height of the nitrogen-induced Snoek-like peak experiences a remarkable increase after pre-straining at temperatures corresponding to well-developed DSA-regime of plastic deformation. The peak increase is probably caused by nitrogen-enriched zones forming by nitrogen–dislocation interactions in the DSA-regime of the material's deformation. Dependence of the nitrogen-induced IF peak decay on time of annealing at the peak temperature corresponds to exponential decay with characteristic time of 9.3 ± 0.6 ks, which probably reflects the post–pre-straining nitrogen re-distribution at scales of the enriched zones of about 0.04–0.1 μm.

Though post-mortem TEM cannot directly observe solute interactions with dislocations, the observed long-range planarity in the dislocation structures at 400 °C, and short-range planarity at 288 °C, in conjunction with the serrations observed in the tensile stress–strain curves, implies that the mechanism of DSA is operating in the material. DSA affects the deformation behaviour of the material by restricting cross-slip and therefore promoting strain localization. The work has demonstrated that DSA is present in commercial AISI 316 NG steel, and may even occur at temperatures relevant to nuclear power plant operation.

References

[1] P. Rodriguez, Bull. Mater. Sci. 6 (1984) 653–663.
[2] S.-G. Hong, S.-B. Lee, J. Nucl. Mater. 328 (2004) 232–242.
[3] S.-G. Hong, S.-B. Lee, J. Nucl. Mater. 340 (2005) 307–314.
[4] S.-G. Hong, S.-B. Lee, T.-S. Byun, Mater. Sci. Eng. A 457 (2007) 139–147.
[5] I.S. Kim, S.S. Kang, Int. J. Pressure Vessels & Piping 62 (1995) 123–129.
[6] U. Ehrnstén, M. Ivanchenko, V. Nevdacha, Y. Yagozinskyy, A. Toivonen, H. Hänninen, Proc. of 12th Int. Conf. on Env. Deg. of Mat. in Nuclear Power Systems – Water Reactors, TMS, 2005, pp. 1475–1482.
[7] A.W. Sleeswyk, Acta Metall. 6 (1958) 598–603.
[8] R.A. Mulford, U.F. Kocks, Acta Metall. 27 (1979) 1125–1134.
[9] M. Gerland, R. Alain, B. Ait Saadi, J. Mendez, Sci. Eng. A 229 (1997) 68–86.
[10] U. Ehrnstén, A. Toivonen, Y. Yagozinskyy, H. Hänninen, Dynamic strain ageing of deformed nitrogen alloyed AISI 316 stainless steels, VTT Research Report TUO73-044670, 2005, p. 39.
[11] M. Ivanchenko, U. Ehrnstén, V. Nevadacha, Y. Yagodzinskyy, H. Hänninen, Proc. of the 7th Int. Conf. on High Nitrogen Steels 2004, GRIPS media GmbH, Ostend, Belgium, September 19–22, 2004, pp. 641–649.
[12] M. Ivanchenko, Y. Yagodzinskyy, H. Hänninen, Mat. Sci. Eng. A (2009), doi:10.1016/j.msea.2008.09.093.
[13] K.M. Rosin, B.N. Finkelshtein, Dok. Acad. Nauk SSSR 91 (1953) 811–814.
[14] M.S. Blanter, I.S. Golovin, H. Neuhäuser, H.-R. Sinning, Internal Friction in Metallic Materials, Springer-Verlag, Berlin, Heidelberg, 2007 (p. 539).
[15] V.D. Verner, Fiz. Tverdogo Tela 7 (1965) 2318–2323.
[16] J.A. Slane, C. Wolverton, R. Gibala, Mater. Sci. Eng. A 370 (2004) 67–72.
[17] A.H. Heuer, F. Ernst, H. Kahn, A. Avishai, G.M. Michal, D.J. Pitchure, R.E. Ricker, Scr. Mater. 56 (2007) 1067–1070.
[18] Yu. Jagodzinski, S. Smouk, A. Tarasenko, H. Hänninen, Proc. of the 5th Int. Conf. on High Nitrogen Steels '98, Espoo, Finland, May 24–26, and Stockholm, Sweden, May 27–28, 1998. Trans Tech Publication Ltd., Switzerland, pp. 47–52.
[19] M. Ivanchenko, V. Nevdacha, Y. Yagodzinskyy, H. Hänninen, Mat. Sci. Eng. A 442 (2006) 458–461.
[20] M. Grujicic, W. Owen, Acta Metall. Mater. 43 (1995) 4201–4211.
[21] A.S. Nowick, B.S. Berry, Anelastic Relaxation in Crystalline Solids, Academic Press, N.Y. London, 1972 (p. 677).
[22] M. Grujicic, J.-O. Nilsson, W.S. Owen, T. Thorvaldsson, Proc. of the Int. Conf. on High Nitrogen Steels '88, Lille, France, May 18–20, 1988. The Institute of Metals, London, pp. 151–158.
[23] Y. Yagodzinskyy, E. Andronova, M. Ivanchenko, H. Hänninen, Mat. Sci. Eng. A (2009), doi:10.1016/j.msea.2008.09.092.
[24] M.E. Glicksman, Diffusion in Solids: Field Theory, Solid-State Principles, and Applications, John Wiley & Sons, Inc., 2000.